Theoretical Studies of Proton Transfers. 1. The Potential Energy Surfaces of the Identity Reactions of the First- and Second-Row Non-Metal Hydrides with Their Conjugate Bases

Scott Gronert

Contribution from the Department of Chemistry and Biochemistry, San Francisco State University, San Francisco, California 94132

Received May 3, 1993®

Abstract: High-level *ab initio* calculations are used to investigate the potential energy surfaces of the identity proton transfers between CH_4, NH_3, OH_2, FH, SiH_4, PH_3, SH_2, and ClH and their conjugate bases. Energies are reported at the MP4/6-311+G(d,p)//MP2/6-31+G(d,p) and G2+ levels. At the highest level, there is a good correlation between the calculated and experimental proton affinities of the conjugate bases (average error, ±0.5 kcal/mol). The proton-transfer potential energy surfaces vary from single wells with stable, symmetric intermediates (FH) to double wells with significant central barriers (CH_4, NH_3, SiH_4, and PH_3). In some systems, a barrier exists on the electronic potential energy surface but disappears when vibrational energy corrections are applied (OH_2, SH_2, and ClH). Considering the full series, it is clear that for a given acidity, the second-row systems face much larger barriers to proton transfer than the first-row analogs. The surfaces are also investigated with Bader's electron density analysis approach. Integrated populations and critical point densities are reported for the complexes and transition structures at the MP2/6-31+G-(d,p) level. In addition, Laplacian representations of the density are shown for the transition structures. The energetics of the potential energy surfaces are discussed in terms of the electron density distributions.

Introduction

Proton transfers involving anionic species represent some of the simplest and most fundamental reactions in chemistry. Although they have been the subject of numerous studies, there is still much to be learned about the details of their potential energy surfaces. Over the years, condensed phase studies have led to important generalizations about proton-transfer barriers.[1] It is well known that proton transfers between electronegative centers (*i.e.*, N, O, F, and Cl, etc.) are usually facile and if exothermic, may have rates near the collision-controlled limit. In contrast, proton transfers involving carbon acids are generally slow, especially if a delocalized carbanion is formed.

Gas-phase studies offer an attractive alternative for studying proton-transfer processes. In the absence of solvation and ion pairing, the rate is completely dependent on the interactions between the acid and the base. Flowing afterglow (FA), ion cyclotron resonance (ICR), and high-pressure mass spectrometric (HP-MS) studies have led to rate constants for a wide variety of proton-transfer reactions.[2] In accord with condensed phase work, it has been observed that heteroatoms give fast proton transfers whereas delocalized carbanions yield much slower reactions by comparison. In addition, there is recent evidence that proton transfers involving second-row elements have larger barriers than those of first-row analogs.[3-4] Although similar trends are observed, the dynamics of gas-phase proton transfers are fundamentally different than those observed in solution. In the case of an anionic system, the base is a bare, unsolvated ion. As the acid approaches, a long-range electrostatic attraction (either ion–dipole or induced dipole) leads to the formation of an energized complex (see Figure 1). This ion–dipole complex can dissociate to give reactants or pass over the barrier to give an ion–dipole complex of the products. The product complex can then dissociate to yield the observed proton-transfer products. Fundamentally, the activation barrier could be defined in two ways: as the energy difference between the initial complex and the transition state ($\Delta E_{barrier}$) or as the energy difference between the free reactants and the transition state (ΔE_{TS}). Although some previous theoretical studies have chosen the former approach,[5] the latter is more appropriate for comparisons to experimental systems. Given the pressures, reaction times, and complex lifetimes typically found in ICR's and FA's, three-body collisions are relatively unlikely, and therefore, the initial, activated ion–dipole complex undergoes little or no collisional stabilization.[6] Because the complex retains its internal energy, its ability to pass through the

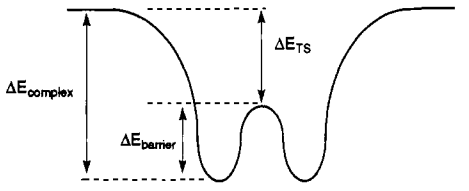

Figure 1. Generalized potential energy diagram for gas-phase ion–molecule reactions.

• Abstract published in *Advance ACS Abstracts*, September 15, 1993.

(1) (a) Koch, H. F. *Acc. Chem. Res.* **1984**, *17*, 137. (b) *Proton Transfer Reactions*; Caldin, E. F., Gold, V., Ed.; Chapman and Hall: London, 1975. (c) Cram, D. J. *Fundamentals of Carbanion Chemistry*; Academic Press: New York, 1973. (d) Streitwieser, A., Jr.; Juaristi, E.; Nebenzahl, L. L. In *Comprehensive Carbanion Chemistry*; Buncel, Durst, T., Eds.; Elsevier: Amsterdam, 1980. (e) Davies, M. H.; Robinson, B. H.; Keeffe, J. R. *Ann. Rep. A* **1973**, 123. (f) Bell, R. P. *The Proton in Chemistry*; Cornell University Press: Ithaca, NY, 1973.

(2) For example, see: (a) Ervin, K. M.; Gronert, S.; Barlow, S. E.; Gilles, M. K.; Harrison, A. G.; Bierbaum, V. M.; DePuy, C. H.; Lineberger, W. C.; Ellison, G. B. *J. Am. Chem. Soc.* **1990**, *112*, 5750. (b) Grabowski, J. J.; DePuy, C. H.; Van Doren, J. M.; Bierbaum, V. M. *J. Am. Chem. Soc.* **1985**, *107*, 7384. (c) Mackay, G. I.; Betowski, L. D.; Payzant, J. D.; Schiff, H. I.; Bohme, D. K. *J. Phys. Chem.* **1976**, *80*, 2919. (d) Bohme, D. K.; Lee-Ruff, E.; Young, L. B. *J. Am. Chem. Soc.* **1972**, *94*, 5153. (e) Brauman, J. I.; Han, C.-C. *J. Am. Chem. Soc.* **1989**, *111*, 6491. (f) Meyer, F. K.; Pellerite, M. J.; Brauman, J. I. *Helv. Chim. Acta* **1981**, *64*, 1058. (g) Farneth, W. E.; Brauman, J. I. *J. Am. Chem. Soc.* **1976**, *98*, 7891. (h) Ikonomou, M. G.; Sunner, J.; Kebarle, P. *J. Phys. Chem.* **1988**, *92*, 6308. (i) Meot-Ner, M.; Field, F. H. *J. Am. Chem. Soc.* **1978**, *100*, 1356. Magnera, T. F.; Kebarle, P. In *Ionic Processes in the Gas Phase*; Alister-Ferreira, A. M., Ed.; NATO ASI Series C; Reidel: Dodrecht, 1982. (j) Lifshitz, C.; Wu, R. L. C.; Tiernan, T. O. *J. Am. Chem. Soc.* **1978**, *100*, 2040.

(3) Gronert, S. *J. Am. Chem. Soc.* **1991**, *113*, 6041.

(4) (a) DePuy, C. H.; Gronert, S.; Mullin, A.; Bierbaum, V. M. *J. Am. chem. Soc.* **1990**, *112*, 8650. (b) Gronert, S.; DePuy, C. H.; Bierbaum, V. M. *J. Am. Chem. Soc.* **1991**, *113*, 4009. (c) Damrauer, R.; Kass, S. R.; DePuy, C. H. *Organometallics* **1988**, *7*, 637.

(5) Cao, H. Z.; Allavena, M.; Tapia, O.; Evleth, E. M. *J. Phys. Chem.* **1985**, *89*, 1581.

(6) *Gas Phase Ion Chemistry*; Bowers, M. T., Ed.; Academic Press: New York, 1979; Vol. I.

0002-7863/93/1515-10258$04.00/0

transition state is related to the energy of the free reactants. Therefore, ΔE_{TS} represents the experimentally observed proton-transfer activation energy. ΔE_{TS} can be either positive or negative, depending on the relative values of $\Delta E_{complex}$ and $\Delta E_{barrier}$.

Theory provides another approach for studying the potential energy surfaces of solvent-free proton transfers. Computational studies have the advantage that they yield not only the energies, but also the structures of the intermediates and the transition states. In addition, the calculations lead directly to activation energies and are not dependent on, or limited by, a dynamics model for correlating rates with barriers.[7-9] In the past, *ab initio* techniques have been used to profile the potential energy surfaces of a variety of simple proton-transfer processes involving anionic bases.[5,10-15] Using modest basis sets at the Hartree–Fock level, Evleth and co-workers[5] have presented a systematic study of proton transfers between CH_4, NH_3, H_2O, HCCH, and HCN and their conjugate bases. In a series of detailed studies, Scheiner and co-workers[10-13] have profiled the potential energy surfaces of proton transfers mainly involving oxygen, nitrogen, and sulfur bases. In addition, *ab initio* studies have been used to characterize a number of anionic acid–base complexes.[16,17]

In the present study, we use high-level *ab initio* calculations to probe the potential energy surfaces of a series of simple proton transfers. Specifically, the identity reactions of the first- and second-row non-metal hydrides (CH_4, NH_3, OH_2, FH, SiH_4, PH_3, SH_2, and ClH) with their conjugate bases are examined.

$$AH_n + {}^-AH_{n-1} \rightarrow {}^-AH_{n-1} + AH_n$$

$$A = C, N, O, F, Si, P, S, \text{or Cl}$$

The series spans a wide range of acidities and central atom electronegativities and, therefore, provides a good basis for generalizations. In addition, these systems yield proton-transfer potential energy surfaces that span the full range from double wells with large central barriers to single wells with stable intermediates. Finally, the series provides the intrinsic barriers required for future studies of the applicability of the Marcus equation to gas-phase proton transfers.[5,12,14,18]

Although a few of the first-row systems have been investigated by high-level *ab initio* calculations in the past,[5,10,11] little work has been reported on the second-row systems. Moreover, relatively few proton-transfer systems have been studied with correlated wave functions.[13] The present results indicate that correlation corrections are needed to properly characterize the *structures and energies* of the species on the proton-transfer potential energy surface.

Calculations

Ab initio calculations were completed using the GAUSSIAN90[19] and GAUSSIAN92[20] quantum mechanical packages as well as GAMESS.[21] Geometries were optimized using 6-31G(d,p) (neutrals) or 6-31+G(d,p) (anions) basis sets[22] at the Hartree–Fock and MP2 levels. At the Hartree–Fock level, the character of all minima and transition states was confirmed with analytical second derivatives. Relative energies are corrected for zero-point vibrations (Hartree–Fock values scaled by 0.9).[23] Frozen-core Moeller–Plesset calculations were completed up to the MP4(SDTQ)/6-311+G(d,p) level using the MP2/6-31+G(d,p) geometries. In some of the calculations, the basis sets of the conjugate bases of the hydrides were augmented with a set of hydrogen functions placed at the approximate position of the missing proton (counterpoise)—the functions are centered at a point in space that best matches the X–H bond lengths and angles found in the parent hydride. At the highest level of theory, the reaction energies were converted to enthalpies at 298 K by standard methods employing the *ab initio* vibrational frequencies.[24]

A modified G2 approach was also taken.[25] Using the MP2/6-31+G(d,p) geometries, single-point calculations were completed at the MP4/6-311+G(2df,p), QCISD(T)/6-311+G(d,p), and MP2/6-311+G(3df,2p) levels. Using the MP4/6-311+G(2df,p) level as a starting point, a correction was made for higher level correlation (ΔE(QCI))

$$\Delta E(\text{QCI}) = [\text{QCISD(T)/6-311+G(d,p)}] - [\text{MP4/6-311+G(d,p)}]$$

and basis set enhancement (ΔE(3df,2p)).

$$\Delta E(\text{3df,2p}) = [\text{MP2/6-311+G(3df,2p)}] - [\text{MP2/6-311+G(2df,p)}]$$

The energies were also corrected for zero-point vibrations (ΔE(ZPE)). In addition, an empirical, higher level correlation (ΔE(HLC)) correction based on the number of paired and unpaired electrons was made. ΔE(HLC) = −0.00481(no. of β valence electrons) − 0.00019(no. of α valence electrons) in hartrees ($\alpha \geq \beta$). The G2+ energy is the sum of these corrections:

$$\text{G2+} = \text{MP4/6-311+G(2df,p)} + \Delta E(\text{QCI}) + \Delta E(\text{3df,2p}) + \text{ZPE} + \Delta E(\text{HLC})$$

As outlined above, a counterpoise approach was used in calculating proton affinities and reaction energies.

Calculations were completed on three types of machines: a Multiflow-Trace 14 at the California State University Computational Chemistry Center, a cluster of Hewlett-Packard 720 workstations at the San Francisco State University Computational Chemistry and Visualization Center, or a Hewlett-Packard 730 workstation.

Electron Density Analysis. Electron density analysis was completed using Bader's approach with a modified version of the PROAIM program.[26] Primitive cutoffs were used in the integrations. Electron density analysis was completed at the HF/6-31+G** and MP2/6-31+G**

(7) (a) Lim, K. F.; Brauman, J. I. *J. Chem. Phys.* **1991**, *94*, 7164. (b) Olmstead, W. N.; Brauman, J. I. *J. Am. Chem. Soc.* **1977**, *99*, 4219. (c) Pellerite, M. J.; Brauman, J. I. *J. Am. Chem. Soc.* **1983**, *105*, 2672.

(8) Chesnavich, W. J.; Bass, L.; Su, T.; Bowers, M. T. J. *J. Chem. Phys.* **1981**, *74*, 2228.

(9) (a) Tucker, S. C.; Truhlar, D. G. *J. Am. Chem. Soc.* **1990**, *112*, 3338. (b) Tucker, S. C.; Truhlar, D. G. *J. Phys. Chem.* **1989**, *93*, 8138.

(10) (a) Cybulski, S. M.; Scheiner, S. *J. Am. Chem. Soc.* **1987**, *109*, 4199. (b) Cybulski, S. M.; Scheiner, S. *J. Am. Chem. Soc.* **1989**, *111*, 23. (c) Cybulski, S. M.; Scheiner, S. *J. Phys. Chem.* **1989**, *93*, 6565. (d) Hillenbrand, E. A.; Scheiner, S. *J. Am. Chem. Soc.* **1985**, *107*, 7690. (e) Scheiner, S.; Bigham, L. D. *J. Chem. Phys.* **1985**, *82*, 3316. (f) Scheiner, S. *J. Chem. Phys.* **1982**, *77*, 4039.

(11) Isaacson, A. D.; Wang, L.; Scheiner, S. *J. Phys. Chem.* **1993**, *97*, 1765.

(12) Scheiner, S.; Redfern, P. *J. Phys. Chem.* **1986**, *90*, 2969.

(13) Luth, K.; Scheiner, S. *J. Chem. Phys.* **1992**, *97*, 7507, 7519.

(14) Donnella, J.; Murdoch, J. R. *J. Am. Chem. Soc.* **1984**, *106*, 4724. (b) Murdoch, J. R. *J. Am. Chem. Soc.* **1983**, *105*, 2159.

(15) For example, see: (a) Jaroszewski, L.; Lesyng, B.; Tanner, J. J.; McCammon, A. *Chem. Phys. Lett.* **1990**, *175*, 282. (b) Roszak, S.; Kaldor, U.; Chapman, D. A.; Kaufman, J. J. *J. Phys. Chem.* **1992**, *96*, 2123.

(16) For example, see: (a) Del Bene, J. E.; Frisch, M. J.; Pople, J. A. *J. Phys. Chem.* **1985**, *89*, 3669. (b) Del Bene, J. E. *J. Comput. Chem.* **1989**, *10*, 603. (c) Mizuse, S.; Hiraoka, K.; Yamabe, S.; Nakatsuji, Y. *Chem. Phys. Lett.* **1988**, *148*, 497.

(17) (a) Sannigrahi, A. B.; Kar, T.; Nandi, P. K. *Chem. Phys. Lett.* **1992**, *198*, 67. (b) Frisch, M. J.; Del Bene, J. E.; Binkley, J. S.; Schaefer, H. F., III *J. Chem. Phys.* **1986**, *84*, 2279.

(18) Marcus, R. A. *J. Phys. Chem.* **1968**, *72*, 891.

(19) Frisch, M. J.; Head-Gordon, M.; Trucks, G. W.; Foresman, J. B.; Schlegel, H. B.; Raghavachari, K.; Robb, M.; Binkley, J. S.; Gonzalez, C.; DeFrees, D. J.; Fox, D. J.; Whiteside, R. A.; Seeger, R.; Melius, C. F.; Baker, J.; Martin, R. L.; Kahn, L. R.; Stewart, J. J. P.; Topiol, S.; Pople, J. A. GAUSSIAN90; Gaussian, Inc.: Pittsburgh, PA, 1990.

(20) Frisch, M. J.; Trucks, G. W.; Head-Gordon, M.; Gill, P. M. W.; Wong, M. H.; Foresman, J. B.; Johnson, B. D.; Schlegel, H. B.; Robb, M. A.; Replogle, E. S.; Gomperts, R.; Andres, J. L.; Raghavachari, K.; Binkley, J. S.; Gonzalez, C.; Martin, R. L.; Fox, D. J.; DeFrees, D. J.; Baker, J.; Stewart, J. J. P.; Pople, J. A. GAUSSIAN92; Gaussian, Inc.: Pittsburgh, PA, 1992.

(21) Schmidt, M. W.; Boatz, J. A.; Baldridge, K. K.; Koseki, S.; Gordon, M. S.; Elbert, S. T.; Lam, B. GAMESS. *QCPE Bull.* **1978**, *7*, 115.

(22) All basis sets were taken from the GAUSSIAN92 program. For details, see: Hehre, W. J.; Radom, L.; Schleyer, P. v. R.; Pople, J. A. *Ab Initio Molecular Orbital Theory*; Wiley-Interscience: New York, 1986.

(23) Pople, J. A.; Schlegel, H. B.; Krishnan, R.; DeFrees, D. J.; Binkley, J. S.; Frisch, M. J.; Whiteside, R. A.; Hout, R. F.; Hehre, W. J. *Int. J. Quantum Chem. Symp.* **1981**, *15*, 269.

(24) Lewis, G. N.; Randall, M.; Pitzer, K. S.; Brewer, L. *Thermodynamics*; McGraw-Hill: New York, 1961.

(25) (a) Curtiss, L. A.; Raghavachari, K.; Trucks, G. W.; Pople, J. A. *J. Chem. Phys.* **1991**, *94*, 7221. (b) Curtiss, L. A.; Jones, C.; Raghavachari, K.; Trucks, G. W.; Pople, J. A. *J. Chem. Phys.* **1990**, *93*, 2537. (c) Pople, J. A.; Head-Gordon, M.; Fox, D. J.; Raghavachari, K.; Curtiss, L. A. *J. Chem. Phys.* **1989**, *90*, 5622.

(26) For recent descriptions, see: (a) Bader, R. F. W. *Acc. Chem. Res.* **1985**, *18*, 9. (b) Bader, R. F. W.; Nguyen-Dang, T. T. *Adv. Quantum Chem.* **1981**, *14*, 63. (c) Wiberg, K. B.; Bader, R. F. W.; Lau, C. D. H. *J. Am. Chem. Soc.* **1987**, *109*, 985.

Table I. Energies and Proton Affinities of Hydrides and Their Conjugate Bases[a]

						proton affinities					
structure	HF	MP2	MP3	MP4	ZPE[c]	HF	MP2	MP3	MP4	298 K	exp[b]
CH_4	-40.20909	-40.37943	-40.39845	-40.40514	26.7						
CH_3^-	-39.51901	-39.70312	-39.71666	-39.72623	17.0	423.3	414.7	418.1	416.3	417.8	416.4 ± 0.7
d	-39.51797	-39.69783	-39.71129	-39.72081	17.0	424.0	418.0	421.5	419.7	421.2	
NH_3	-56.21417	-56.41520	-56.42614	-56.43424	20.8						
NH_2^-	-55.54211	-55.76089	-55.76258	-55.77736	11.3	412.2	401.0	406.9	402.7	404.2	404.0 ± 0.3
d	-55.54117	-55.75530	-55.7570	-55.77141	11.3	412.8	404.6	410.4	406.4	407.9	
OH_2	-76.05243	-76.27471	-76.27732	-76.28703	13.1						
OH^-	-75.40610	-75.64679	-75.63802	-75.65714	5.2	397.7	386.1	393.3	387.4	388.6	390.5 ± 0.3
d	-75.40505	-75.64000	-75.63079	-75.64988	5.2	398.3	390.4	397.8	391.9	393.1	
HF	-100.05257	-100.27877	-100.27674	-100.28611	5.8						
F^-	-99.44614	-99.68548	-99.67382	-99.69190	0.0	374.8	366.6	372.6	367.2	368.1	371.4 ± 0.2
d	-99.44566	-99.67869	-99.66690	-99.68443	0.0	375.1	370.8	377.0	371.8	372.7	
SiH_4	-291.25321	-291.37212	-291.39533	-291.40161	18.8						
SiH_3^-	-290.64017	-290.76378	-290.78643	-290.79335	11.7	377.6	374.7	375.0	374.6	376.0	373.0 ± 0.9
d	-290.64004	-290.75903	-290.7810	-290.78776	11.7	377.7	377.6	378.4	378.1	379.5	
PH_3	-342.47788	-342.61299	-342.63539	-342.64202	14.6						
PH_2^-	-341.87977	-342.01815	-342.03735	-342.04426	7.5	368.2	366.2	368.2	368.0	369.5	368.2 ± 0.5
d	-341.87943	-342.01112	-342.02996	-342.03659	7.5	368.5	370.6	372.8	372.8	374.3	
SH_2	-398.70205	-398.84747	-398.86641	-398.87198	9.2						
SH^-	-398.13563	-398.28043	-398.29559	-398.30151	3.6	349.9	350.3	352.7	352.4	353.6	351.4 ± 0.7
d	-398.13547	-398.27330	-398.28774	-398.29352	3.6	349.9	354.7	357.5	357.4	358.7	
ClH	-460.09533	-460.24469	-460.25974	-460.26357	4.1						
Cl^-	-459.56559	-459.71080	-459.72219	-459.72624	0.0	328.4	331.0	333.3	333.1	334.0	333.5 ± 0.1
d	-459.56543	-459.70357	-459.71428	-459.71816	0.0	328.5	335.5	338.2	338.2	339.1	

[a] Geometries from optimizations at the MP2/6-31G(d,p) (neutrals) and MP2/6-31+G(d,p) (anions) levels. Energies calculated with a 6-311+G(d,p) basis set. In the calculations of anions, a set of hydrogen orbitals is placed at the position of the missing proton (see text). Energies in hartrees and proton affinities in kcal/mol. [b] Reference 31a. [c] Scaled by 0.9. [d] Calculations without an additional set of hydrogen orbitals (standard 6-311+G(d,p)).

levels (diffuse functions were ommitted for neutral compounds). The application of Bader's approach has been discussed in detail elsewhere,[26] so only a brief description is provided here. The n_X values represent the integrated densities within the zero-flux surfaces surrounding atom X in the molecular wave function. They provide rigorously-defined, physically meaningful measures of the charges on each of the atoms. Previous work has shown that this approach is far superior to conventional Mulliken population analysis.[27] The ρ value is the density at the critical point of a bond where the critical point is defined as the density minimum along the bond path connecting the two atoms.

In earlier work, it has been shown that relative ρ values provide a reasonable measure of the bond order.[28,29] However, the absolute value of ρ is dependent on the size of the atoms, and comparisons between different bonding partners is difficult. Finally, Bader has shown that the Laplacian of the electron density ($\nabla^2\rho$) is a useful tool for characterizing bonding interactions.[26] Regions where the Laplacian is negative correlate with electronic charge concentration and in the interatomic region are characteristic of covalent bonding interactions. Regions where the Laplacian is positive correlate with charge depletion and indicate areas where the electron density has contracted toward the nuclei. Little shared density and only a weak covalent interaction are anticipated in these regions. In the present study, contour representations of the Laplacian were generated using the MACGRIDZO program.[30]

Results

Proton Affinities. A good test of the theoretical model is its ability to characterize the proton affinities of the deprotonated hydrides.[31] In Table I, gas-phase proton affinities have been tabulated at a variety of levels. At the MP4 level (corrected to 298 K), there is a reasonable correlation (average error, ±4 kcal/mol) between the theoretical and experimetnal values; however, several systems give results that are unsatisfactory. Specifically, errors of greater than 5 kcal/mol result for the proton affinities of SiH_3^-, SH^-, and Cl^-. Better values are obtained if a counterpoise approach is taken, that is, in the calculation of the anion, an additional set of hydrogen orbitals is added to the basis set and placed at the approximate position of the mising proton. In Table I, values from the counterpoise calculations are also listed. Although the added functions have almost no effect on the Hartree–Fock energies, they provide a significant improvement to the correlated energies. Apparently, in some cases, the diffuse functions of the 6-31+G** basis set do not adequately describe the virtual orbitals of the Hartree–Fock wave function and therefore provide a poor basis for the perturbation theory. After the counterpoise corrections, the theoretical values are much closer to the experimental proton affinities—the average error is ±1.8 kcal/mol. Further improvement is realized by adopting a modified version (G2+) of Pople and co-workers' G2 approach (Table II).[25] In short, energies are calculated at the MP4(SDTQ)/6-311+G(2df,p) level, and corrections are made for higher correlation levels (QCISD(T)) and expansion of the basis set (6-311+G(3df,2p)). In the original description of the method, Pople and co-workers reported average errors of 1.2 kcal/mol for a vareity of systems.[25] The calculations in the present study employed slightly larger basis sets for the optimizations. Neutrals were optimized at the MP2/6-31G(d,p) level and anions at the MP2/6-31+G(d,p) level instead of using the standard G2 approach of MP2/6-31G(d). In addition, diffuse functions were used in the QCISD(T) calculation (6-311+G(d,p) instead of 6-311G(d,p)) because anions were involved. Moreover, the counterpoise approach was applied to the calculation of the conjugate bases. With our G2+ approach, the average error is reduced to ±0.5 kcal/mol.[32] The accuracy of these calculations provides strong support for our theoretical method and suggests

(27) For example, see: (a) Bachrach, S. M.; Streitwieser, A., Jr. *J. Am. Chem. Soc.* **1984**, *106*, 2283. (b) Bachrach, S. M.; Streitweiser, A., Jr. *J. Comput. Chem.* **1989**, *10*, 514. (c) Gronert, S.; Glaser, R.; Streitwieser, A., Jr. *J. Am. Chem. Soc.* **1989**, *111*, 3111.

(28) For example, see: (a) Knop, O.; Boyd, R. J.; Choi, S. C. *J. Am. Chem. Soc.* **1988**, *110*, 7299. (b) Bader, R. F. W.; Slee, T. S.; Cremer, D.; Kraka, E. *J. Am. Chem. Soc.* **1983**, *105*, 5061.

(29) In the text, critical point densities are reported in units of e/au^3.

(30) MacGRIDZO; Rockware; Inc.: Wheat Ridge, CO.

(31) (a) Proton affinities in the text are derived from a thermodynamic cycle, ΔH_{acid} = BDE(H–AH_{n-1}) + IP(H·)-EA($^-AH_{n-1}$); see: Berkowitz, J.; Ellison, G. B.; Gutman, D. Personal communication. *J. Phys. Chem.*, accepted for publication. (b) Values derived from equilibrium measurements are from Lias, S. G.; Bartmess, J. E.; Liebman, J. F.; Holmes, J. L.; Levin, R. D.; Mallard, W. G. *J. Phys. Chem. Ref. Data* **1988**, *17*, Supplement no. 1.

(32) The values from the present G2+ level are relatively similar to those found at the standard G2 level. An average deviation from experiment of ±0.8 kcal/mol is observed using the data from Smith, B. J.; Radom, L. *J. Phys. Chem.* **1991**, *95*, 10549.

Table II. G2+ Energies and Proton Affinities of Non-Metal Hydrides and their Conjugate Bases[a]

structure	MP4/ 6-311+G(2df,p)	MP2/ 6-311+G(2df,p)	MP2/ 6-311+G(3df,2p)	QCISD(T)/ 6-311+G(d,p)	HLC	G2+	proton affinity 0 K	298 K	expt[b]
CH_4	–40.42488	–40.39795	–40.40570	–40.40599	–0.02	–40.41092			
CH_3^-	–39.74708	–39.72316	–39.73180	–39.72653	–0.02	–39.74892	415.4	416.9	416.4 ± 0.7
NH_3	*–56.46224*	*–56.44167*	*–56.45058*	*–56.43453*	*–0.02*	*–56.45828*			
NH_2^-	–55.80560	–55.78826	–55.79894	–55.77599	–0.02	–55.81689	402.5	404.0	404.0 ± 0.3
OH_2	–76.32324	–76.30905	–76.31827	–76.28662	–0.02	–76.33116			
OH^-	–75.69270	–75.68113	–75.69114	–75.65380	–0.02	–75.71108	389.1	390.3	390.5 ± 0.3
FH	–100.33121	–100.32152	–100.32943	–100.28520	–0.02	–100.34896			
F^-	–99.73586	–99.72780	–99.73521	–99.68779	–0.02	–99.75916	370.1	371.0	371.4 ± 0.2
SiH_4	–291.42200	–291.38910	–291.39404	–291.40351	–0.02	–291.41887			
SiH_3^-	–290.81714	–290.78394	–290.79027	–290.79519	–0.02	–290.82666	371.6	373.0	373.0 ± 0.9
PH_3	–342.67372	–342.64003	–342.64680	–342.64379	–0.02	–342.67899			
PH_2^-	–342.07849	–342.04772	–342.05680	–342.04355	–0.02	–342.09490	366.5	368.0	368.2 ± 0.5
SH_2	–398.91675	–398.88582	–398.89322	–398.87310	–0.02	–398.93060			
SH^-	–398.34946	–398.32245	–398.33136	–398.30218	–0.02	–398.37330	349.7	350.9	351.4 ± 0.7
ClH	–460.31937	–460.29212	–460.29876	–460.26416	–0.02	–460.34006			
Cl^-	–459.78462	–459.76140	–459.76773	–459.72667	–0.02	–459.81138	331.8	332.7	333.5 ± 0.1

[a] See text for description of the G2+ method. Absolute energies in hartrees. Proton affinities in kcal/mol. [b] Values from ref 31a. Equilibrium measurement values from ref 31b: NH_3, 403.6 ± 0.8; SiH_4, 372.3 ± 2.0; PH_3, 370.9 ± 2.0; and SH_2, 351.2 ± 2.1.

that our modified G2 approach should be adequate for the purposes of the present study. In an earlier study, Gordon *et al.*[33] reported proton affinities (average deviation = ±0.8 kcal/mol) at the MP4-(SDTQ)/6-311++G(3df,2pd) level.[34]

Finally, it should be noted that there is a significant discrepancy between the calculated (*ab initio* and thermodynamic cycle[31a]) proton affinities (368.0 and 368.2 kcal/mol, respectively) of PH_2^- and the value determined *via* gas-phase equilibrium measurements (370.9 kcal/mol).[31b] Given the reliability of the G2+ approach and the small uncertainties associated with the derived proton affinities,[31a] it appears that the equilibrium value[31b] is too large by about 3 kcal/mol.

Potential Energy Surfaces. The structures of the complexes and the transition states of the first-row systems are given in Figure 2. Those for the second-row systems are given in Figures 3 and 4. For all of the systems, the energies are listed in Tables III and IV, and the results of the Bader analysis are given in Table V.

First-Row Systems. CH_3^- + CH_4. With a ΔH_{acid} of 416.4 kcal/mol, CH_4 is the least acidic of the hydrides in this study. given that there is little polarization in the C–H bonds, it is not surprising that the CH_3^-/CH_4 system exhibits a small complexation energy (–0.9 kcal/mol at 298 K). Using Bader's approach to determining charge densities, an integrated population (n_H) of near unity (1.03 e) is found for the hydrogens of CH_4 and a ρ value of 0.281 is calculated for the C–H bonds. The complex **1C** has C_s symmetry and an exceptionally long distance between the carbanion and the nearest methane hydrogen, 2.62 Å (Figure 2). From this weak complex, the system passes through a D_{3d} symmetric transition state, **1TS**, with C–H bond distances of 1.43 Å to the transferring hydrogen. The weakness of the bridging C–H bonds is evidenced by the relatively small ρ value (0.127). The population of the transferring hydrogen is 0.70 e, and in response to the carbanion character, the populations of the remaining hydrogens increase to 1.13 e. At the G2+ level, the transition state lies 9.3 kcal/mol above the separated reactants. For comparison, Evleth and co-workers[5] found a similar structure but a much higher transition-state energy (23.5 kcal/mol) in their 6-31G* calculations. More recently in a dynamics study,

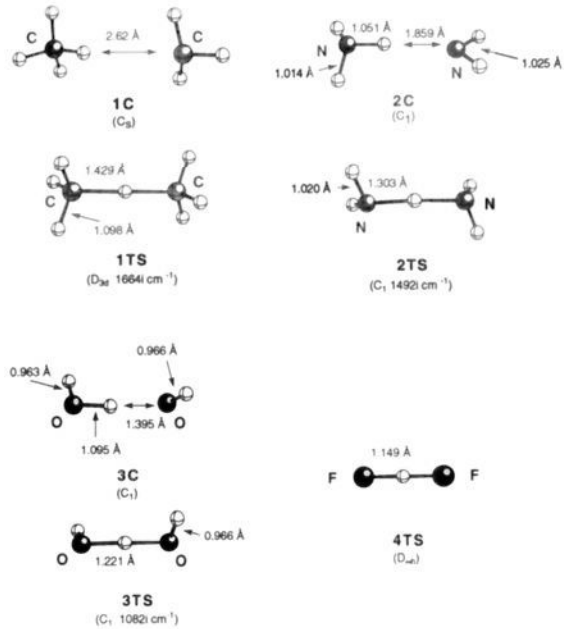

Figure 2. Structures of first-row complexes and transition structures (MP2/6-31+G(d,p)). Symmetry and imaginary frequency given parenthetically.

Scheiner and co-workers examined the potential energy surface at the 4-31G level and found a transition-state energy of 1.4 kcal/mol.[12]

NH_2^- + NH_3. The polarity of the N–H bonds in NH_3 (n_H = 0.65) leads to a reasonably strong hydrogen-bonding interaction with NH_2^- (complexation energy = –11.7 kcal/mol). The complex **2C** exhibits C_1 symmetry and an $NH_2^-\cdots H–NH_2$ bond length of 1.86 Å at the MP2/6-31+G** level (2.01 Å at the HF/6-31+G** level). At the highest level of theory, a barrier of less than 2 kcal/mol separates the degenerate hydrogen-bonded complexes. This places the transition state **2TS** at an energy of –10.5 kcal/mol with respect to the separated reactants, and therefore, proton transfer should occur readily under typical gas-phase reaction conditions. For comparison, Evleth and co-workers[5] found a complexation energy of –12.6 kcal/mol and a transition-state energy of –7.1 kcal/mol at the 4-31+G level. Experimentally, Grabowski *et al.*[2b] have observed an efficient hydrogen–deuterium exchange reaction for NH_2^- + ND_3 and ND_2^- + NH_3.[2b] In the transition state, the population on the transferring hydrogen drops to 0.48 e whereas that of the

(33) Gordon, M. S.; Davis, L. P.; Burggraf, L. W.; Damrauer, R. *J. Am. Chem. Soc.* **1986**, *108*, 7889.

(34) (a) Recently, Del Bene has examined the effect of basis set contraction on proton affinity calculations; see: Del Bene, J. *J. Phys. Chem.* **1993**, *97*, 107. (b) In earlier work, Pople and Schleyer also examined proton affinities; see: Pople, J. A.; Schleyer, P. v. R.; Kaneti, J.; Spitznagel, G. W. *Chem. Phys. Lett.* **1988**, *145*, 359. (c) DeFrees has reported very high level calculations on HF, H_2O, and NH_3; see: DeFrees, D. J.; McLean, A. D. *J. Comput. Chem.* **1986**, *7*, 321.

remaining hydrogens rises to 0.74 e. The ρ value of the N–H bond decreases from 0.343 in NH_3 to 0.152 in the transition state.

OH^- + OH_2. This system has been the subject of several previous studies.[5,10c,35] Because the O–H bond is highly polarized (n_H = 0.42 e) in H_2O, the resulting acid–base complex **3C** is characterized by strong hydrogen bonding and a large complexation energy (–25.3 kcal/mol). In the complex, O–H bond lengths of 1.40 and 1.10 Å are observed. As in the previous systems, a longer hydrogen-bonding distance is observed at the Hartree–Fock level (1.56 Å). Experimentally, Kebarle recently has measured a complexation energy of –27.6 kcal/mol for this system.[36] Although a transition state for proton transfer, **3TS**, can be lcoated on the electronic potential energy surface, it disappears when zero-point energy corrections are applied—the corrected energy for **3TS** is 2.5 kcal/mol below that of **3C**. In the complex, the HO–H–OH potential is exceptionally anharmonic and in fact, the proton-transfer barrier is below the zero-point vibrational level. As a result, the reaction of HO^- with H_2O effectivley leads to a symmetric complex with a very shallow potential for distortion along the O–H–O reaction coordinate. Given that **3TS** is the lowest energy species on the potential energy surface, it is more appropriate to compare its energy (–27.8 kcal/mol)[37,38] with the expeirmental complexation energy (–27.6 kcal/mol).[36] An efficient hydrogen–deuterium exchange is also observed in the reaction of $D^{18}O^- + H_2O$.[2b]

In the transition state, the bridging and free hydrogens have integrated populations of 0.37 and 0.50 e, respectively. The ρ value for the bridging bond is 0.164 as compared to 0.368 in H_2O.

F^- + HF. The large charge polarization in HF (n_H = 0.29 e) leads to a very strong complex with F^-. Complex **4TS** is symmetric and contains H–F bond lengths of 1.14 Å. In this case, the electronic potential energy surface does not contain a barrier to proton transfer and the symmetric species is a minimum. The lowest frequency vibration corresponds to the proton-transfer motion and has a frequency of 616 cm^{-1}. Complex **4TS** has an energy of –44.1 kcal/mol with respect to those of the separated reactants. In a recent study, Sannigrahi *et al.*[17a] found a complexation energy of 40.7 kcal/mol at the MP4/6-311+G(d) level. In earlier, high-level theoretical work, Frisch and co-workers found a complexation energy of 45 kcal/mol.[17b] Experimentally, a complexation energy of 38.6 kcal/mol has been measured.[39]

Second-Row Systems. SiH_3^- + SiH_4. Of the second-row systems, silane (ΔH_{acid} = 373.0 kcal/mol) is the weakest acid. In contrast to the first-row systems, the Si–H bond is polarized with the hydrogen bearing a significant negative charge (n_H = 1.72 e). As a result, hydrogen bonding to an anion would lead to a repulsive interaction. When SiH_3^- is allowed to interact with SiH_4, a weak complex is formed, **5C** (Figure 3). It involves the interaction of the SiH_3^- lone pair with the backside of one of the silane's Si–H bonds (C_{3v} symmetry) and is characterized by a long Si–Si distance (3.88 Å). This distance is very sensitive to correlation corrections, and at the HF/6-31+G** level, a distance of 4.47 Å is observed. When zero-point energy and correlation effects are included, the calculations predict that the formation of **5C** is endothermic at the MP4 level. With the added corrections of the G2+ level, **5C** becomes ~2.5 kcal/mol more stable than the reactants. Pentacoordinate complexes formed by the addition of the SiH_3^- to the silicon of SiH_4 are also possible.

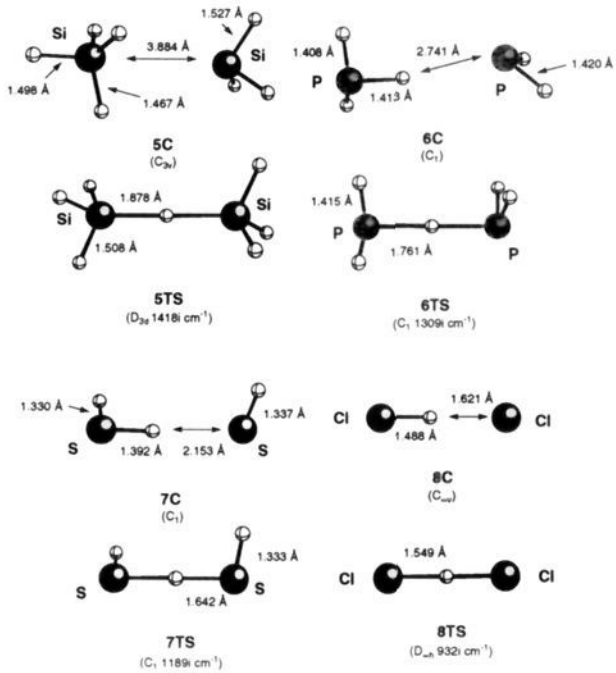

Figure 3. Structures of second-row complexes and transition structures (MP2/6-31+G(d,p)). Symmetry and imaginary frequency given parenthetically.

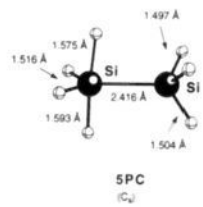

Figure 4. Pentacoordinate complex found for SiH_3^- + SiH_4. Symmetry given parenthetically.

The pentacoordinate complex with the SiH_3 group in the axial position is unstable and decomposes without a barrier to **5C**; however, the structure with an equatorial SiH_3, **5PC** (Figure 4), is a stable minimum on the potential energy surface. It is characterized by a relatively long Si–Si distance (2.42 Å) and is 1.7 kcal/mol less stable than the reactants at the G2+ level. In earlier work at the 6-31G* level, Gordon *et al.*[33] found a similar structure for the equatorial complex.

From complex **5C**, the silicon system can undergo proton transfer *via* a D_{3d} symmetric transition state, **5TS**. The transition state has Si–H bond lengths of 1.91 Å and involves a barrier of 12.3 kcal/mol with respect to those of the separated reactants. Although the reaction is formally a proton transfer, the transferring hydrogen maintains a population of greater than unity (1.11 e) in the transition state. The ρ value for the transferring Si–H bond is 0.075 as compared to 0.118 in SiH_4.[40]

PH_2^- + PH_3. PH_3 is slightly more acidic (ΔH_{acid} = 368.2 kcal/mol) than SiH_4. As in the silicon system, the bonds to hydrogen are polarized with excess density on the hydrogens (n_H = 1.57 e). The complex formed between PH_2^- and PH_3 has C_1 symmetry and a long-range H_2P^-–HPH_2 interaction (2.74 Å at MP2/6-31+G** and 3.06 Å at the HF/6-31+G** level). As in the silicon system, when correlation and zero-point energies are included, the complex **6C** becomes less stable than the reactants at the MP4 level. However, a small complexation energy (–3.3 kcal/mol) is found at the G2+ level. Obviously, the MP4/6-

(35) Gao, J.; Garner, D. S.; Jorgensen, W. L. J. *J. Am. Chem. Soc.* **1986**, *108*, 4784 and references therein.

(36) Paul, G. J. C.; Kebarle, P. *J. Phys. Chem.* **1990**, *94*, 5184 and references therein.

(37) The frequency associated with the shuttling of the proton is ignored in this analysis (it corresponds to the imaginary frequency of the supposed transition state). This frequency should be relatively low, and only a small error is anticipated (<1 kcal/mol); see ref 38.

(38) (a) Kreevoy, M. M.; Liang, T. M. *J. Am. Chem. Soc.* **1980**, *102*, 3315. (b) Eliason, R.; Kreevoy, M. M. *J. Am. Chem. Soc.* **1978**, *100*, 7037.

(39) Larson, J. W.; McMahon, T. B. *Inorg. Chem.* **1984**, *23*, 2029.

(40) Proton transfer can also be completed *via* the pentacoordinate complex **5PC**. A full discussion of this pathway is presented elsewhere; see: Gronert, S. *Organometallics*, in press.

311+G(d,p) calculations are not adequate to describe the subtle bonding forces in these complexes. From **6C**, the system passes through transition state **6TS** to complete the proton-transfer process. The transition state has C_1 symmetry, and the distance between the phosphorous and the transferring proton is 1.76 Å. The relative energy of this transition state is −1.4 kcal/mol at the G2+ level. A C_s symmetric transition state is also possible, but it is slightly less stable (by 0.3 kcal/mol) at the 6-31+G** level. In the transition state, the transferring hydrogen has a slightly positive charge (n_H = 0.96 e) and the P–H ρ value is reduced from 0.161 to 0.092.

HS^- + H_2S. H_2S is a much stronger acid (ΔH_{acid} = −351.1 kcal/mol) than silane or phosphine. In addition, the hydrogens have a much smaller partial negative charge (n_H = 1.12 e). When HS^- interacts with H_2S, a complex, **7C**, is formed with an HS^-–HSH bond distance of 2.15 Å (2.48 Å at the Hartree–Fock level). In contrast to the complexes formed in the phosphorous and silicon systems, **7C** is significantly more stable than the reactants (complexation energy = ~11 kcal/mol). The transition state for proton transfer **7TS** is similar to that found in the HO^-/H_2O system and incorporates S–H bond lengths of 1.64 Å to the transferring hydrogen. As in the HO^-/H_2O system, the symmetric species is slightly more stable than the complex once zero-point energy corrections are included. Therefore, the proton transfer does not involve a barrier, and the reaction of HS^- with H_2S should lead to a symmetric complex with a very shallow well with respect to distortion along the S–H–S coordinate. Experimentally, hydrogen–deuterium exchange is observed in the reaction of DS^- with H_2S.[2b] In the transition structure, the transferring proton has a significant positive charge (n_H = 0.75) and the shared density in the S–H bond is reduced (ρ value = 0.110 as compared to 0.218 in H_2S).

Cl^- + HCl. HCl is by far the most acidic species (ΔH_{acid} = 333.5 kcal/mol) in both series. Unlike the F^-/HF system, a complex does exist on the electronic potential energy surface at the present level of theory. The geometry of complex **8C** is sensitive to the level of theory, and the Cl-H hydrogen-bonding distance contracts from 2.03 Å (HF/6-31+G**) to 1.62 Å (MP2/6-31+G**) when correlation is included. The proton-transfer transition state is linear and has a Cl–H distance of 1.55 Å. The transition state **8TS** is 23.3 kcal/mol more stable than the reactants. As expected, the barrier to proton transfer disappears when zero-point energy corrections are made and **8TS** becomes ~2 kcal/mol more stable than **8C**. The energy of the symmetric species compares favorably with previous theoretical (−23.5 kcal/mol)[17a] and experimental (−21.8 kcal/mol)[39] values.

Discussion

Double-Well vs Single-Well Potentials. Although double-(multi) well potentials are commonly observed in gas-phase ion–molecule reactions, some of the proton transfers in this study involve single-well potentials.[6] That is, a symmetric complex is formed without activation. The conversion from double-well to single-well behavior is clearly seen by considering the series: CH_4, NH_3, H_2O, and HF. In the CH_4/CH_3^- system, a weak complex is formed and there is little hydrogen bonding. In going from the complex to the symmetric species, extensive geometry changes occur (the C–C distance shrinks from 3.66 to 2.91 Å) and the normally covalent C–H bond is forced to accept ionic character. Consequently, there is a barrier, and a typical double-well potential is observed. In the NH_3/NH_2^- system, hydrogen bonding leads to a tighter complex so less extensive geometry changes occur in the conversion to the symmetric transition state **2TS**—the N–N distance contracts from 2.91 to 2.61 Å. In addition, the greater electronegativity difference between N and H allows for more ionic bonding. The net result is a double-well potential with a small barrier (Figure 5a). The strong hydrogen bonding in the H_2O/HO^- system leads to a complex, **3C**, whose interoxygen distance is very similar to that of the symmetric species **3TS** (2.50 vs 2.44 Å), that is, the double-well potential is beginning to coalesce to give a single well. As the proton moves between the oxygens, there is a small barrier on the electronic potential energy surface (at least at G2+); however, this barrier is below the zero-point energy level of the H–O bond (Figure 5b). Kreevoy[38] has discussed this situation in the past. Although the potential energy surface exhibits a maximum, the O–H–O coordinate can be treated as a normal, bound vibration where the proton oscillates between oxygens with every vibration. Therefore, the H_2O/HO^- system can be treated as a single, symmetric complex in which the position of the central hydrogen cannot be localized. In the HF/F^- system, extensive polarization of the HF bond leads to a very strong hydrogen-bonding interaction. This system is best characterized by an ionic model where the central proton is flanked by two fluorides. This results in a single-well potential (Figure 5c) where the proton is equally shared.

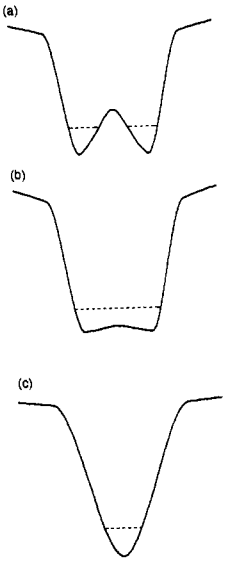

Figure 5. (a) Double-well potential with barrier above ground-state vibrational level; (b) Double-well potential with barrier below ground-state vibrational level; and (c) Single-well potential. The dashed line indicates the lowest vibrational level.

Activation Energies. From the energies in Tables III and IV, it is clear that calculations at the G2+ level result in more stable complexes and transition states (by ~3–5 kcal/mol) than those at the MP4/6-311+G(d,p) level. Given the reliability of the G2+ results (see above), the rest of the discussion will focus on these values. Although the potential energy surfaces vary from single to double wells in this series, for the following discussion, the term transition structure will be used indiscriminately to describe the symmetric species on the surface.[41]

First-Row vs Second-Row Systems. It is reasonable to assume that there should be a correlation between the acidities of the hydrides and their barriers to proton transfer. In Figure 6, the energies of the transition structures are plotted against the proton affinities of the conjugate bases. The plot cleanly breaks into two sets of lines. The first-row hydrides give a good correlation (r^2 = 0.979) with a slope of 1.16. Therefore, increases in acidity are amplified in the stabilization of the transition structure. The data indicate that for these thermoneutral proton transfers, strong acid/weak base combinations are kinetically preferred. In terms of the Marcus equation,[18] the stronger acids have the lowest intrinsic barriers to proton transfer.

The second-row systems give a separate correlation with the acidity of the hydride. There is more curvature in the data (r^2

(41) Tunneling may play a significant role in these proton transfers. To quantitatively assess the importance of tunneling, a full dynamics study is required. For example, see ref 11.

Table III. Energies of Complexes and Transition States[a]

structure		HF	MP2	MP3	MP4	relative energies[b] ZPE[c]	HF	MP2	MP3	MP4	298 K
CH_3^- CH_4	1C	-79.72917	-80.08211	-80.11459	-80.13105	44.4	0.0	0.9	1.0	0.8	1.2
CH_3–H–CH_3^-	1TS	-79.69433	-80.06231	-80.09274	-80.11042	41.3	19.0	10.5	11.8	11.0	10.4
NH_2^- NH_3	2C	-111.77437	-112.19555	-112.20762	-112.23052	33.8	-9.6	-10.5	-10.1	-10.2	-9.3
NH_2–H–NH_2^-	2TS	-111.75995	-112.18935	-112.19983	-112.22352	31.2	-3.0	-9.0	-7.7	-8.2	-9.4
OH^- OH_2	3C	-151.49455	-151.95943	-151.95256	-151.98090	20.3	-20.9	-22.1	-21.6	-21.3	-22.7
HO–H–OH^-	3TS	-151.49267	-151.95918	-151.95202	-151.98044	17.8	-21.9	-24.1	-23.5	-23.2	-25.0
F–H–F	4TS	-199.5640	-200.02803	-200.01453	-200.03994	5.8	-41.0	-40.0	-40.1	-38.8	-39.8
SiH_3^- SiH_4	5C	-581.89515	-582.13690	-582.18238	-582.19560	31.0	-0.7	-0.2	0.0	0.0	0.6
SiH_3–H–SiH_3^-	5TS	-581.85201	-582.10739	-582.15207	-582.16602	28.1	23.8	15.7	16.4	16.0	16.2
H_4Si–SiH_3^- (eq)	5PC	-581.87444	-582.12532	-582.16986	-582.18342	31.6	13.0	7.7	8.5	8.3	6.9
PH_2^- PH_3	6C	-684.36036	-684.63263	-684.67352	-684.68698	23.0	-0.9	-0.1	0.3	0.4	1.1
PH_2–H–PH_2^-	6TS	-684.33778	-684.62306	-684.66178	-684.67608	21.2	11.7	4.3	6.1	5.7	5.2
SH^- SH_2	7C	-796.84977	-797.14164	-797.17369	-797.18546	14.0	-6.5	-7.6	-6.3	-6.5	-6.8
HS–H–SH^-	7TS	-796.84075	-797.14075	-797.17139	-797.18361	12.0	-2.7	-8.8	-6.6	-7.1	-8.0
Cl^- ClH	8C	-919.68521	-919.98495	-920.00832	-920.01657	4.9	-14.5	-17.8	-15.8	-16.1	-17.0
Cl–H–Cl^-	8TS	-919.68495	-919.98505	-920.00835	-920.01662	2.8	-16.2	-19.7	-17.7	-18.0	-19.1

[a] Geometries in the MP2/6-31+G(d,p) level. Energies calculated with 6-311+G(d,p) basis set. Absolute energies in hartrees and relative energies in kcal/mol. [b] Relative to the free reactants, AH_{n+1} + AH_n^-. Energies reference to the anions (AH_n^-) calculated with counterpoise correction (see text). [c] kcal/mol scaled by 0.9.

Table IV. G2+ Energies of Complexes and Transition States[a]

structure		MP4/ 6-311+G(2df,p)	MP2/ 6-311+G(2df,p)	MP2/ 6-311+G(3df,2p)	QCISD(T)/ 6-311+G(d,p)	HLC	G2+	relative energy 0 K	298 K
CH_3^- CH_4	1C	-80.17440	-80.12324	-80.14033	-80.13231	-0.04	-80.16196	-1.3	-0.9
CH_3–H–CH_3^-	1TS	-80.15349	-80.10351	-80.11901	-80.11128	-0.04	-80.14401	9.9	9.3
NH_2^- NH_3	2C	-112.28934	-112.25164	-112.27046	-112.22960	-0.04	-112.29335	-11.4	-11.7
NH_2–H–NH_2^-	2TS	-112.28321	-112.24637	-112.26396	-112.22249	-0.04	-112.29003	-9.3	-10.5
OH^- OH_2	3C	-152.05834	-152.03355	-152.05115	-151.97766	-0.04	-152.08034	-23.9	-25.3
HO–H–OH^-	3TS	-152.05802	-152.03344	-152.05088	-151.97706	-0.04	-152.08370	-26.0	-27.8
FHF^-	4TS	-200.13607	-200.11970	-200.13357	-200.03616	-0.04	-200.17691	-43.1	-44.1
SiH_3^- SiH_4	5C	-582.24422	-582.17788	-582.19002	-582.19938	-0.04	-582.25072	-3.3	-2.7
SiH_3–H–SiH_3	5TS	-582.21604	-582.14955	-582.16109	-582.16953	-0.04	-582.22629	12.1	12.3
H_4Si–SiH_3^- (eq)	5PC	-582.23489	-582.16955	-582.18192	-582.18708	-0.04	-582.24054	3.1	1.7
PH_2^- PH_3	6C	-684.75821	-684.69399	-684.70968	-684.69008	-0.04	-684.78033	-4.0	-3.3
PH_2–H–PH_2^-	6TS	-684.75111	-684.68866	-684.70383	-684.67890	-0.04	-684.77530	-0.9	-1.4
SH^- SH_2	7C	-797.28508	-797.22844	-797.24450	-797.18740	-0.04	-797.32076	-10.6	-10.9
HS–H–SH^-	7TS	-797.28466	-797.22946	-797.24437	-797.18538	-0.04	-797.32221	-11.5	-12.4
Cl^- HCl	8C	-920.13902	-920.09125	-920.10265	-920.01748	-0.04	-920.18351	-20.1	-21.0
Cl–H–Cl^-	8TS	-920.13912	-920.09142	-920.10272	-920.01753	-0.04	-920.18687	-22.2	-23.3

[a] See text for description of the G2+ method. Absolute energies in hartrees. Relative energies in kcal/mol.

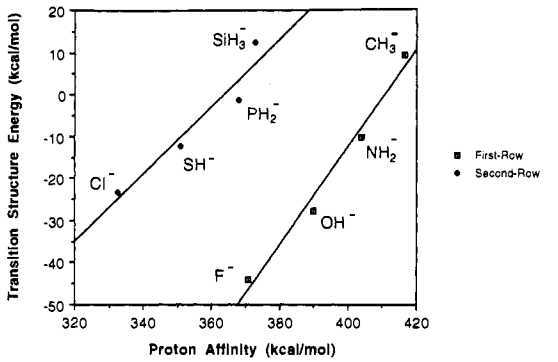

Figure 6. Plot of transition-structure energy vs proton affinity of the conjugate base. Energies at the G2+ level.

= 0.922), and a smaller slope value (0.86) is observed. However, the most important difference is the displacement of the line. It is shifted in such a way that second-row systems are associated with much larger barriers than first-row systems of comparable acidity. For example, SiH_4 and FH have similar gas-phase acidities (373.0 vs 371.4 kcal/mol), yet the relative stabilities of their transition structures (**5TS** and **4TS**) differ by over 50 kcal/mol (12.3 vs -44.1 kcal/mol). This clearly points to a strong kinetic bias against proton transfer in the second-row systems.

Bond Polarizations. Another approach to analyzing the barriers is to consider the polarization of the X–H bonds in the hydrides. This can be accomplished by using the Bader method to determine the integrated hydrogen populations in each of the hydrides. Presumably, if there is a large polarization in the X–H bond, strong hydrogen bonds will be formed. In turn, this should stabilize the proton-transfer transition state. By examining the values in Table V, a clear difference is seen between the first- and second-row hydrides.[42] For all of the first-row systems with the exception of CH_4, the hydrogen populations are less than unity, indicating that the hydrogens bear a partial positive charge. This allows for hydrogen bonding in the complex and suggests a favorable charge distribution in the transition state. For the case of HF, the polarization is extensive and the system is perfectly poised to adopt a "triple-ion" structure for the symmetric complex.

$$\overset{-}{F}\text{–}\overset{+}{H}\text{–}\overset{-}{F}$$

For the second-row hydrides, all of the n_H values, except one (HCl), are greater than unity, indicating that the hydrogens have excess density. Because the hydrogens have partial negative charges, their interactions with anions are repulsive and, therefore, hydrogen bonding is not energetically favorable.

$$\overset{\delta^+}{H}_3Si\text{–}\overset{\delta^-}{H} \qquad \overset{\delta^+}{H}_2P\text{–}\overset{\delta^-}{H}$$

For SiH_4 and PH_3, this effect leads to the formation of exceedingly weak complexes without any significant hydrogen-

(42) Boyd has noted the advantages of using correlated wave functions for Bader analyses; see: Shi, Z.; Boyd, R. J. *J. Am. Chem. Soc.* **1991**, *113*, 1072.

Table V. Critical Point Densities and Integrated Populations from Bader Analysis[a]

structure	bond	ρ (HF)[b]	ρ (MP2)[c]	atom	n(HF)[b]	n(MP2)[c]
CH_4	C–H	0.286	0.281	H	1.06	1.03
CH_3^- CH_4	C–H[d]	0.005	0.005	H[d]	0.95	0.93
CH_3–H–CH_3^-	C–H	0.122	0.127	H[d]	0.61	0.70
				C	6.12	6.26
				H	1.19	1.13
NH_3	N–H	0.358	0.343	H	0.62	0.65
NH_2^- NH_3	N–H[d]	0.026	0.037	H[d]	0.44	0.48
NH_2–H–NH_2^-	N–H	0.149	0.152	H[d]	0.4	0.48
				N	8.3	8.28
				H	0.74	0.74
H_2O	O–H	0.391	0.368	H	0.38	0.42
HO^- H_2O	O–H[d]	0.060	0.102	H[d]	0.26	0.35
HO–H–OH	O–H	0.165	0.164	H[d]	0.28	0.37
				O	9.39	9.32
				H	0.47	0.5
HF	H–F	0.397	0.372	H	0.24	0.29
F–H–F^-	H–F	0.171	0.169	H	0.10	0.14
				F	9.95	9.93
SiH_4	Si–H	0.118	0.118	H	1.74	1.72
SiH_3^- SiH_4	e					
SiH_3–H–SiH_3	Si–H	0.073	0.075	H[d]	1.05	1.11
				Si	12.09	12.14
				H	1.8	1.77
PH_3	P–H	0.163	0.161	H	1.61	1.57
PH_2^- PH_3	P–H[d]	0.007	0.014	H[d]	1.57	1.5
PH_2–H–PH_2^-	P–H	0.089	0.092	H[d]	0.88	0.96
				P	14.26	14.3
				H	1.65	1.61
H_2S	S–H	0.223	0.218	H	1.24	1.12
HS^- H_2S	S–H[d]	0.018	0.036	H[d]	0.88	0.84
HS–H–SH^-	S–H	0.105	0.110	H[d]	0.67	0.75
				S	16.31	16.4
				H	1.36	1.22
HCl	Cl–H	0.263	0.257	H	0.77	0.59
Cl^- HCl	Cl–H[d]	0.036	0.102	H	0.57	0.60
Cl–H–Cl	Cl–H	0.117	0.123	H	0.52	0.60
				Cl	17.74	17.70

[a] ρ values in e/au^3. [b] HF/6-31+G(d,p)//HF/6-31+G(d,p). [c] MP2/6-31+G(d,p)//MP2/6-31+G(d,p). [d] Hydrogen-bonded hydrogen. [e] No hydrogen-bonding interaction.

bonding interactions. SiH_4 and PH_3 may be viewed as being composed of central cations (Si or P) surrounded by an exterior of hydride-like hydrogens. For proton transfer to occur, the X–H bond must first reverse its polarization to allow for bonding to the approaching anion. In other words, for the hydrogen to be transferred as a proton, it must first lose its hydride character. This reverse polarization has an energetic cost, and this energy is the cause of the larger intrinsic barriers observed for second-row systems. This argument can also be couched in terms of molecular orbital theory. In a proton transfer, the lone pair of the base interacts with the σ^* orbital of the X–H bond. In typical systems where the central atom X is more electronegative than hydrogen (*i.e.*, the first-row hydrides), the σ-bonding orbital is mainly centered on the X atom and, consequently, the σ^* orbital is mainly centered on the hydrogen. This allows for a favorable orbital interaction between the incoming base and the transferring hydrogen. In the second-row systems such as SiH_4 and PH_3, the polarization of the X–H bond is reversed; consequently, the σ-bonding orbital is mainly centered on the hydrogen, and the σ^* orbital is mainly centered on the central atom X. As a result, the dominant interaction in the proton-transfer process is a repulsive one between the lone pair of the base and the filled σ-bonding orbital of the X–H bond. In the silicon system, the reverse polarization effect is so extensive that a strong interaction between the silyl anion and the σ^* orbital leads to an attack at silicon and the appearance of the complex **5PC**. To obtain a favorable proton-transfer interaction in these reverse polarized systems, the σ-bonding electrons must be promoted into the σ^* orbital. This of course has an energetic cost and is equivalent to reversing the polarity of the X–H bond.[43]

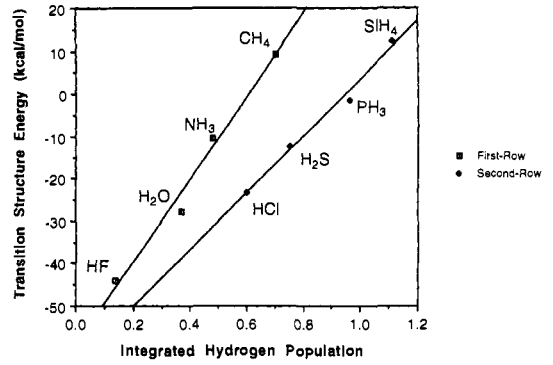

Figure 7. Plot of transition-structure energy vs integrated population of the transferring hydrogen. Energies at the G2+ level and populations from MP2/6-31+G(d,p) wave functions.

In Figure 7, the transition-state energy is plotted against the n_H value of the transferring proton. Again, the plot can be separated into lines for the first- and second-row systems. A strong correlation between charge and transition-state (complex) energy is observed in each case. As expected, more protic character in the hydrogen leads to a more stable transition structure. Because proton transfer is fundamentally an ionic process, systems that can most easily adopt a triple-ion structure, H_nA^- H^+ ^-AH_n, face the smallest barriers.[44]

Electron Density. The bonding in the transition states can be visualized with contour representations of the Laplacian. As noted earlier, negative $\nabla^2\rho$ values indicate charge concentration or, in other words, electron localization. Positive values are related to regions of charge dispersal or contraction toward the nuclei. In Figure 8, contour representations for the transition states (complexes) are shown. The plots are generated from a slice of the Laplacian through the plane containing the X–H–X fragment. In many plots, other X–H bonds also appear in this plane. The heavy atoms are on the left and right sides of the plots and are characterized by a concentration of positive (black) and negative (gray) contours near the nucleus. The transferring proton is at the center of the plot and is outlined by a series of circular, negative (gray) contours. A clear trend is observed in the first-row series from carbon to fluorine. In the CH_4 system, a broad set of negative contours links the transferring proton to the carbons. This is consistent with charge localization in the bonding region and strong covalent interaction. In the NH_3 and OH_2 systems, the breadth of negative contours connecting the heavy atoms to the proton is significantly reduced, indicating a progression toward a more ionic interaction. Finally, in the FH system, the negative contours in the interatomic region disappear and the F and H are separated by a region of positive $\nabla^2\rho$ values, indicating little covalency in the bonding. The shift toward ionic bonding across this series correlates with the increasing stabilities of the transition structures. Plots of the second-row systems yielded a similar trend.

Conclusions

Comparisons with experiment indicate that the G2+ approach provides a reliable method for determining the acidity of the first- and second-row non-metal hydrides and suggests that it is suitable for characterizing the potential energy surfaces of the identity proton transfers in this study. Three general types of potential energy surfaces are observed in these systems. For the least electronegative atoms within each series (C, N, Si, and P), double-well potentials are observed with a central barrier

(43) Similar arguments have been used to explain the large barriers found in E2 eliminations initiated by second-row bases; see ref 3.

(44) Hiraoka has found similar effects with proton-bound dimers; see: Hiraoka, K.; Takimoto, H.; Yamabe, S. *J. Phys. Chem.* **1986**, *90*, 5910.

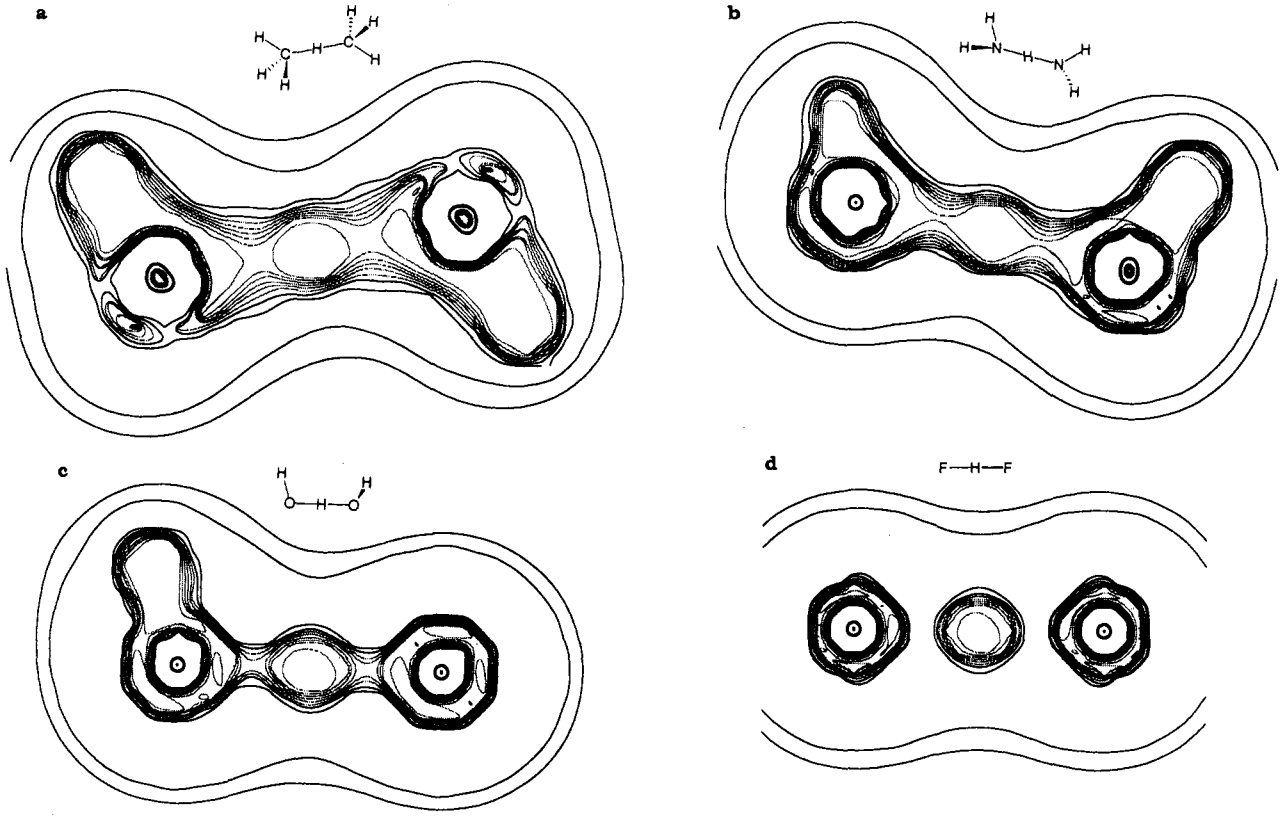

Figure 8. Contour representations of the Laplacians of the transition structures (black, $\nabla^2\rho > 0$; grey, $\nabla p2\rho < 0$). (a) CH_3–H–CH_3^-; (b) NH_2–H–NH_2^-; (c) HO–H–OH^-; and (d) F–H–F^-. Contours from –0.15 to 0.12 au with a step size of 0.03 au.

separating two degenerate ion–dipole complexes. With the more electronegative atoms within each series (O, S, and Cl), there is a small barrier on the electronic potential energy surface but it is below the lowest vibrational level. As a result, these systems involve a symmetric complex. For the most electronegative atom (F), there is no barrier to proton transfer on the electronic potential energy surface and an exceptionally stable, symmetric complex is formed.

For the first- and second-row systems, separate correlations can be made between the energies of the symmetric species (transition states or complexes) and the acidities of the parent hydrides. The results indicate that more acidic hydrides have lower intrinsic barriers to proton transfer and that second-row systems face much larger barriers than first-row systems of comparable acidity.

Acknowledgment. The author wishes to thank the National Science Foundation for its generous financial support (CHE-9208895). The author also thanks Prof. G. Barney Ellison for providing a preprint of his recent review of bond strengths and electron affinities. The author is also indebted to the referees for helpful suggestions concerning the manuscript.

Supplementary Material Available: Lists of *Z* matrix elements, energies, and frequencies (8 pages). Ordering information is given on any current masthead page.